Article

The self-supporting NiMn-LDHs/rGO/NF composite electrode showing much enhanced electrocatalytic performance for oxygen evolution reaction

Jia Wang, Yongfu Lian *

Key Laboratory of Functional Inorganic Material Chemistry, Ministry of Education, School of Chemistry and Materials Science, Heilongjiang University, Harbin 150080, China

* Correspondence: chyflian@hlju.edu.cn (Y.L.)

Abstract: The poor conductivity and instability of layered dihydroxides (LDHs) limit their widespread application in oxygen evolution reaction (OER). In this study, the composite electrode of NiMn-LDHs, reduced graphene oxide (rGO) and nickel foam (NF), i.e., NiMn-LDHs/rGO/NF, was prepared by a hydrothermal method. When subjected to oxygen evolution reaction (OER) catalytic performance in a solution of 1 M KOH, the NiMn-LDHs/rGO/NF composite catalyst exhibited an overpotential of only 140 mV at a current density of 10 mA cm^{-2} and a Tafel slope of 49 mV dec^{-1}, which is not only better than the comparing RuO_2/NF catalyst, but also better than most of the Mn-based and the Ni–Fe containing bimetallic OER catalysts reported in the literature. The excellent electrocatalytic performance is ascribed to the efficient integration of ultrathin NiMn-LDHs sheets, thin-layered rGO and NF, contributing a lot to the decrease in charge transfer resistance and the increase in electrochemically active surface area. Moreover, NF plays a role of current collector and a role of rigid support for the NiMn-LDHs/rGO composite, contributing extra conductivity and stability to the NiMn-LDHs/rGO/NF composite electrode.

Keywords: self-supporting electrode; reduced graphene oxide; layered NiMn-dihydroxide; electrocatalyst; oxygen evolution reaction

1. Introduction

Hydrogen is an efficient and renewable energy resource, which is regarded to be highly promising alternative to fossil fuel. It can help mitigate environmental pollution resulting from the combustion of fossil fuel and meet the energy demand of our rapidly developing society. Among the many methods of hydrogen production, water electrolysis has attracted widespread attention as a high-efficiency and environmentally friendly technology to produce hydrogen. Electrolysis of water is composed of hydrogen evolution reaction (HER) in a two-electron process and oxygen evolution reaction (OER) in a four-electron process[1]. Since the anodic four-electron reaction process of OER is much slower than that of the two-electron reaction process of HER, high overpotential and the sluggish kinetics inevitably occur in the electrolysis of water. Therefore, it is needed to develop an effective electrocatalyst to improve the energy conversion efficiency[2,3]. However, the slow kinetics of the OER presents a significant challenge for the widespread implementation of water electrolysis as a large-scale hydrogen production technology. Therefore, it is crucial to develop an efficient OER catalyst.

LDHs are two-dimensional layered functional materials composed of positively charged hydroxide layers with equilibrium charges of anions between the layers[4].The general chemical formula of LDHs is $[M_{1-x}^{2+}M_x^{3+}(OH)_2]^{x+}[A^{n-}]_{x/n}\cdot zH_2O$, in which z is the number of interlayer water molecules[5]. LDHs, as common catalysts, have a unique two-dimensional layered structure and could

be exfoliated into ultrathin nanosheets, which are characterized with their large specific surface area and are conductive to the improvement in the catalytic performance of LDHs. On the other hand, the metal cations in LDHs materials have variable valence states, which is beneficial for the electron transfer in the catalytic reactions. To date, many LDHs including NiFe-LDHs, FeCo-LDHs, NiCo-LDHs, NiCr-LDHs and NiMn-LDHs have been prepared and applied in the fields of catalysts, adsorption materials, energy storage materials and sensor materials[6-11], etc. Recently, NiMn-LDH was reported to be of quite good catalytic activity in the OER reaction when applied as catalyst in the electrolysis of water[12]. Wang et al. synthesized cobalt-doped NiMn-LDH by hydrothermal method, which exhibited an overpotential of 310 mV and a Tafel slope of 59 mV dec^{-1} at a current density of 10 mA cm^{-2} in alkaline media[13]. Nonetheless, the electrocatalytic performance of LDHs materials is still limited for their poor electrical conductivity and easy agglomeration leaded low surface area (ECSA)[14-17].

Because of its unique ultrathin sheet structure and excellent chemical stability and electrical conductivity, graphene is often integrated with some catalysts to improve their catalytic performance[18]. The composite of cobalt-based metal-organic framework (MOF) and reduced graphene oxide (rGO) synthesized by Yaqoob et al displayed good electrochemical activity with an overpotential of 290 mV at 10 mA cm^{-2}[19]. The composite of graphene and Co_3O_4 prepared by Mao et al demonstrated an improved OER performance owing to the heterojunction created at the interface of graphene sheet and Co_3O_4 nanoparticles[20]. The composite of copper benzodicar boxylate and rGO prepared by Jahan et al was a promising composite catalyst for OER, because of its quite good stability and much low resistance[21]. Han et al. prepared the composite of FeNi-LDH and GO by GO guiding the constructing of FeNi-LDH arrays. When applied as a desirable bifunctional electrocatalyst for the splitting of water, it demonstrated better OER performance than conventional commercial catalyst because of its enhanced conductivity and electronic interactions[22]. Mooni, et al. prepared the bimetal oxides (MnO_2-NiO) and graphene oxide mixed composite electrodes (GO/MnO_2-NiO), which displayed an overpotential of 379 mV and maintained stable for 8 h at 10 mA cm^{-2} when applied in the study of anodic water oxidation activities in an aqueous alkaline solution[23]. Ma et al. firstly synthesized NiMn-LDH nanoplatelets by a hydrothermal treatment of a mixed Ni^{2+}/Mn^{2+} salt solution in the presence of H_2O_2 and hexamethylenetetramine, and then prepared the hetero-assembly of NiMn-LDH nanosheets and GO/rGO through molecular hybridization of the LDH nanosheets with rGO. When applied as electrocatalyst for OER, the face-to-face hetero-assembly of NiMn LDH nanosheets with conductive rGO at an alternating sequence resulted in a small overpotential of 0.26 V and a Tafel slope of 46 mV per decade[24]. Apart from graphene, other carbon materials[25,26], as well as copper and nickel meshes[4,5], are also optical candidates to composite with LDHs to improve their OER performance.

In this study, the composite of NiMn-LDHs and rGO loaded on NF was facilely prepared by a one-pot hydrothermal treatment of a mixed Ni^{2+}/Mn^{2+} salt solution in the presence of urea and NF. When subjected to the test for OER, the as-prepared NiMn-LDHs/rGO/NF displayed extremely low overpotential at 10 mA cm^{-2} and much small Tafel slope, which might be owing to the synergistic effect established between NiMn-LDHs and rGO. rGO prevents the NiMn-LDHs nanosheets from agglomeration, whereas the NiMn-LDHs nanosheets alleviate the graphitization of rGO during hydrothermal process.

2. Results

Shown in **Error! Reference source not found.a & 1b** are the SEM images of NiMn-LDHs/NF and NiMn-LDHs/rGO/NF synthesized by hydrothermal method. It can be seen from **Figure 1a** that the synthesized NiMn-LDHs agglomerate on the surface of NF to form particles as large as 1 μm. In contrast, as displayed in **Figure 1b** the ultra-thin sheets of NiMn-LDHs are cross-linked and assembled vertically and uniformly on the surface of rGO to form nano-walled networks, which is certainly beneficial for the enlargement of the specific area of the synthesized composite electrode. Therefore, rGO plays definitely a role to prevent NiMn-LDHs nanosheets from aggregating together into large particles.

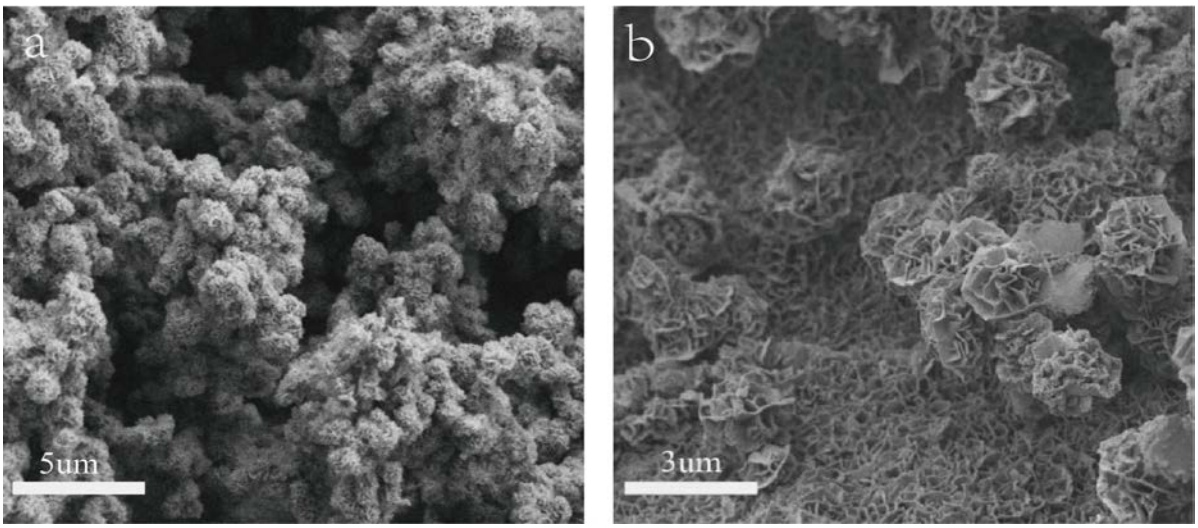

Figure 1. SEM images (a, b) of NiMn- LDHs/NF and NiMn-LDHs/rGO/NF.

TEM observations were applied to investigate the microstructure of the NiMn-LDHs/rGO composite deposited on the inner surface of NF. In the TEM image shown in **Error! Reference source not found.a**, thin rGO sheets are observed with curved brims, whereas the ultra-thin NiMn-LDHs nanosheets are flat and transparent with straight and sharp edges. In the HR-TEM image displayed in **Error! Reference source not found.b**, the lattice fringes of a NiMn-LDHs nanosheet are arranged regularly with a lattice spacing of 0.24 nm, which corresponds perfectly to the (110) crystallographic plane NiMn-LDHs[23]. Moreover, these highly oriented lattice fringes indicate that the synthesized NiMn-LDHs in the NiMn-LDHs/rGO composite are of a long range ordered crystal structure, which is strongly supported by the SAED image shown in Error! Reference source not found.**c**. From the energy dispersive spectroscopy (EDS) elemental mapping image demonstrated in Error! Reference source not found.**d**, it can be seen that the Mn, Ni, C and O elements are homogeneous distributed in the NiMn-LDHs/rGO composite, confirming the successful combination of rGO and NiMn-LDHs sheets.

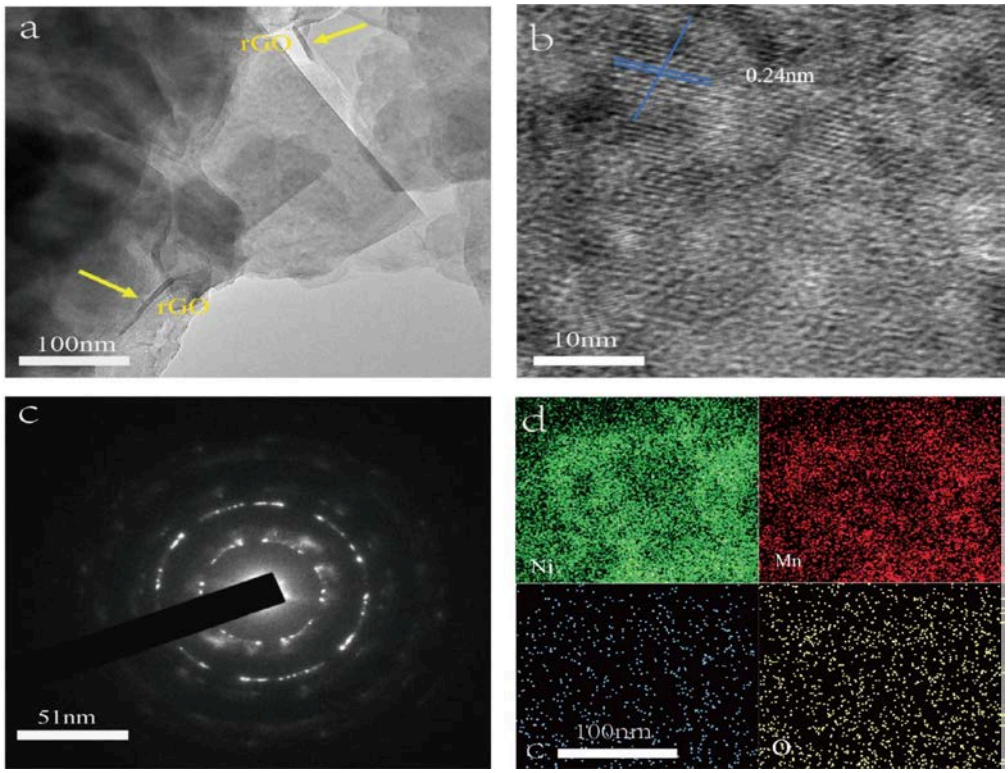

Figure 2. TEM, HR-TEM, SAED and TEM-EDS images (a – d) of NiMn-LDHs/rGO/NF.

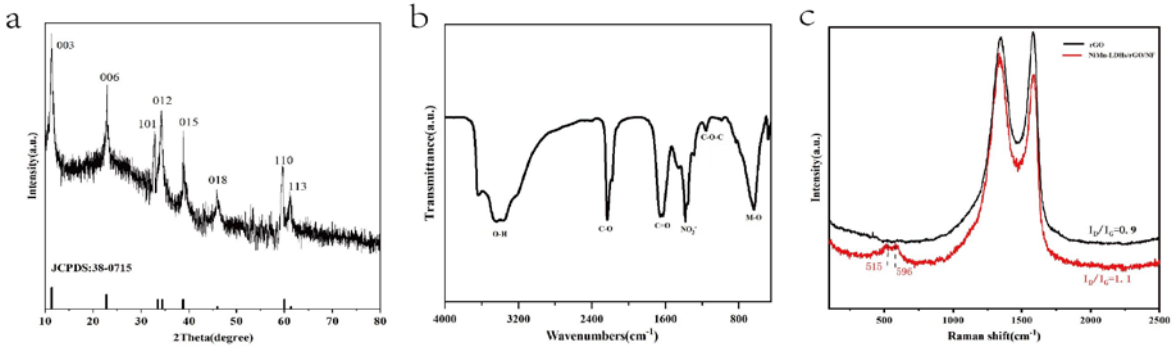

Figure 3. XRD pattern, FT-IR spectrum and Raman spectrum (a-c) of NiMn-LDHs/rGO.

In the X-ray diffraction (XRD) pattern of NiMn-LDHs/rGO shown in **Figure 3a**, the indexed crystal planes of all diffraction peaks correspond to the typically layered structure of hydrotalcite-like materials (NiMn-LDHs: PDF 38-0715), and the broad peak centered around 23° is assigned to rGO. Thus, it is concluded that the NiMn-LDHs sheets integrate with rGO with high purity and crystallinity, and that rGO has little effects on the crystalline structure of NiMn-LDHs. In the Fourier transform infrared (FT-IR) spectrum displayed in **Figure 3b**, the broad band centered around 3432 cm^{-1} is ascribed to the superimposed stretching vibration of hydroxyl groups out of hydrogen-bonded H_2O molecules intercalated between LDHs layers and metal hydroxyl groups in NiMn-LDHs. The strong bands at 640 cm^{-1} could be attributed to the vibrational stretching mode of M-O-M and M-O in hydrotalcite-like materials, and the intense band appeared at 1380 cm^{-1} is recognized to the asymmetric stretching mode of nitrate ions intercalating in the interlayer[22,23]. Whereas, the features located at 2229, 1657 and 1144 cm^{-1} correspond to the C=O stretching, C=O ring stretching and C-O-

 doi:10.20944/preprints202305.0210.v1

C bending vibrations of rGO, respectively. In the Raman spectrum of NiMn-LDHs/rGO demonstrated in **Figure 3c**, the most prominent scattering bands are assigned to the D and G bands of rGO, and the features appeared at 515 and 596 cm^{-1} are ascribed to the symmetric stretching vibrations of disordered (or defected) $Ni(OH)_2$ and MnOOH[27], respectively. In comparison with that of rGO, the intensity ratio of D band to G band (I_D/I_G) is obviously increased. Therefore, upon the formation of the NiMn-LDHs/rGO composite the rGO is well exfoliated and enriched in structural defects, which contributes a lot both to the enlargement of specific surface and to the increase of active sites. In summary, the data shown in Figure 3 confirm strongly that the NiMn-LDHs/ rGO composite was successfully synthesized in the pores of NF[23].

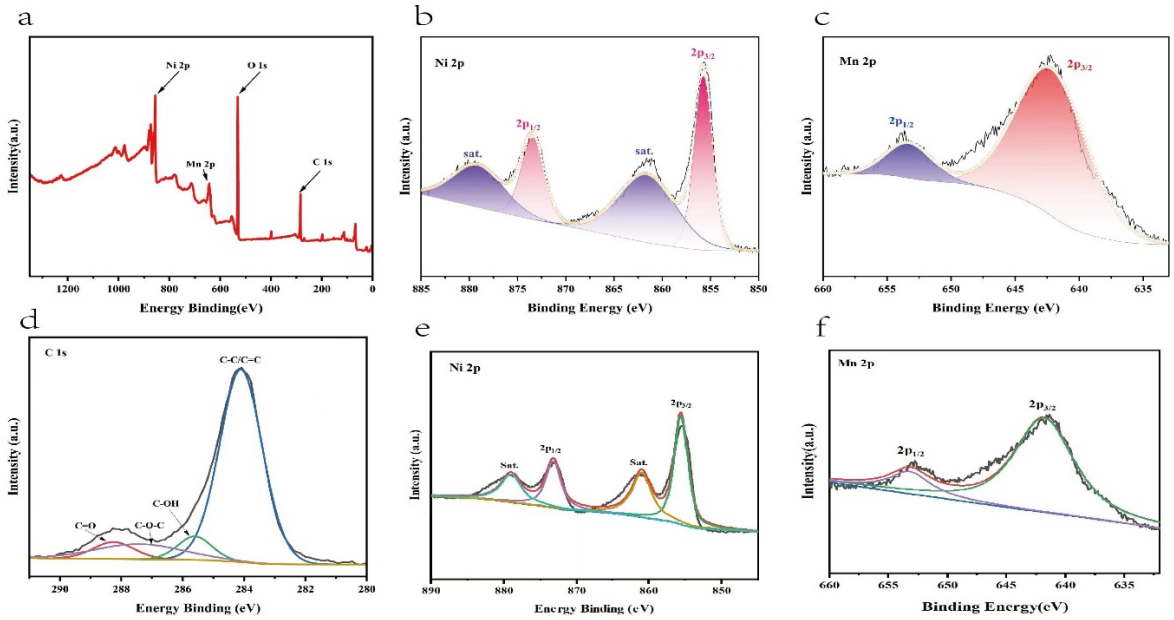

Figure 4. (a-d) The survey, deconvoluted Ni 2p, Mn 2p, C 1s XPS spectra of the NiMn-LDHs/rGO composite.

The surface chemical state and elemental composition of the NiMn-LDHs/rGO composite was investigated by XPS. Illustrated in **Figure 4 a-d** are the survey and deconvoluted Ni 2p, Mn 2p, C 1s and O 2p XPS spectra of the NiMn-LDHs/rGO composite, respectively, along with the deconvoluted Ni 2p and Mn 2p ones of NiMn-LDHs for comparison. From the survey XPS spectrum displayed in **Figure 4a**, it can be seen that elements including Ni, Mn, C and O are present in the NiMn-LDHs/rGO composite, which is consistent with the results of TEM-EDS elemental mapping. In the deconvoluted Ni 2p XPS spectrum (**Figure 4b**), the peaks located at 873.5 and 855.8 eV accompanied by satellites are owing to the $2p_{1/2}$ and $2p_{3/2}$ characteristic peaks of Ni^{2+}[13], respectively, confirming the existence of Ni^{2+} ions. In the deconvoluted Mn 2p XPS spectrum (**Figure 4c**), the peaks located at 653.7 and 642.2 eV are ascribed to the $2p_{1/2}$ and $2p_{3/2}$ characteristic peaks of Mn^{3+}, respectively, indicative of the presence of Mn^{3+} ions. In the deconvoluted XPS C 1s spectrum (**Figure 4d**), the peaks located at 284.1 eV, 285.6 eV, 287.5 eV and 288.3 eV could be attributed to the characteristic features of C-C/C=C, C-OH, C-O-C and C=O bonds, respectively, implying that GO has been partly reduced to rGO. The residual oxygen atoms in rGO play an important role for the charge transfer from the metal ions in NiMn-LDHs to rGO, i.e., the interactions between NiMn-LDHs and rGO contributes a lot to the enhancement of the OER catalytic activity of the NiMn-LDHs/rGO composite. Moreover, in comparison with the features of NiMn-LDHs displayed in **Figure 4e** and **Figure 4f**, the binding

 doi:10.20944/preprints202305.0210.v1

energy of Ni^{2+} and Mn^{3+} of NiMn-LDHs/rGO is positively shifted about 0.4 eV, confirming the charge transfer from the metal ions of NiMn-LDHs to rGO.

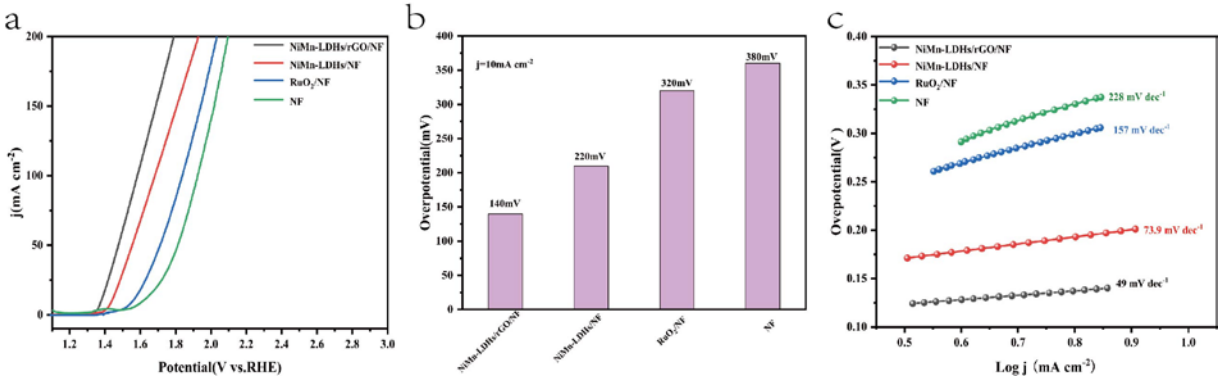

Figure 1. (a) rGO-NiMn-LDHs/NF, NiMn-LDHs/NF, RuO_2/NF, NF OER polarization curve. (b) Tafel diagram of above electrodes. (c) Overpotential diagram of above electrodes at 10mA cm^{-2}.

The electrochemical performance of the NiMn-LDHs/rGO/NF composite electrode along with those of NiMn-LDHs/NF, RuO_2/NF and NF for OER was evaluated in a typical three-electrode system using Hg/HgO and Pt wire as the reference and counter electrodes, respectively, in 1 M aqueous KOH solution. Shown in **Figure 5a** are the iR-corrected linear sweep voltammetry (LSV) curves at a scan rate of 5 mV s^{-1} in the potential range of 1.2−3.0 V (vs. RHE). It is notable that the NiMn-LDHs/rGO/NF electrode exhibits the highest polarization current, which is 1.37 V vs. RHE for achieving a current density of 10 mA cm^{-2}. Moreover, it can be seen from **Figure 5b** that an overpotential as low as 0.14 V is enough for the NiMn-LDHs/rGO/NF electrode to operate at 10 $mAcm^{-2}$ current density, which is lower than those of NiMn-LDHs/NF (0.22 V), RuO_2/NF (0.32 V) and NF (0.38 V) electrodes, evidencing the quite good catalytic efficiency of the NiMn-LDHs/rGO/NF electrode owing to the synergistic effect induced by the direct and interfacial contact between ultrathin NiMn-LDH nanosheets and partly reduced rGO[24].

The Tafel slope represents the reaction kinetics, which is another critical factor for evaluating the performance of a catalyst. As presented in **Figure 5c**, the Tafel slopes of the NiMn-LDHs/rGO/NF, NiMn-LDHs/NF, RuO_2/NF and NF electrodes are 49, 73.9, 157 and 228 mV dec^{-1}, respectively, implying the improved catalytic activity, i.e., the fast reaction kinetics, through the hetero-assembly of NiMn-LDH nanosheets and rGO. On the one hand, rGO can prevent NiMn-LDHs nanoflakes from agglomeration, offer more active sites and accelerate electron migration/transfer for the catalysis. On the other hand, the ultrathin NiMn-LDH sheets also could reduce the graphitization degree of rGO, leading to the increase in the unsaturated sites and in the catalytic activity of the NiMn-LDHs/rGO composite catalyst. More importantly, the charge transfer from Mn and Ni ions of NiMn-LDHs to rGO leads to the increase in the valance state of Mn and Ni ions and the enlargement of charge distribution in rGO, rendering the NiMn-LDHs/rGO composite catalyst to be of the elevated conductivity, the synergistic coupling effect and accordingly the improved electrochemical performance. It should be pointed out that of NiMn-LDHs/rGO/NF composite electrocatalyst outperforms not only RuO_2/NF but also most of the Mn-based and the Ni–Fe containing bimetallic OER catalysts reported in the literature[8,9].

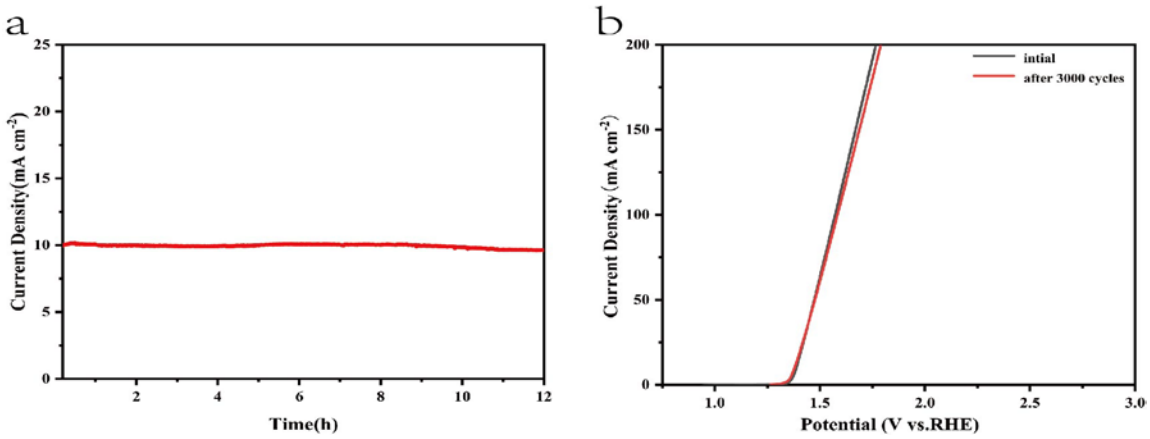

Figure 6. (a) Chronopotentiometry curve of the NiMn-LDHs/rGO/NF electrode at a constant current density of 10 mA cm^{-2}, (b) iR-corrected LSV curves of original catalysts (black line) and after 3000 CV cycles for overall water splitting in 1 M KOH under a current density of 10 mA cm^{-2} (red line).

Moreover, the electrochemical stability is another criterion to evaluate the OER catalysts. A chronopotentiometry test under the current density of 10 mA cm^{-2} was conducted to estimate the stability and durability of the composite electrocatalysts. As shown in **Figure 6a**, the current density of the NiMn-LDHs/rGO/NF electrode was kept nearly constant for 12 h. From **Figure 6b** it can be seen that no obvious change is recorded for the original NiMn-LDHs/rGO/NF electrode and that after 3000 CV cycles under the current density of 10 mA cm^{-2}, indicating that the NiMn-LDHs/rGO/NF composite catalyst has excellent stability and durability in alkaline solution. Such improvement may be a result of the high mechanical strength and electrochemical stability of the NiMn-LDHs/rGO/NF electrode.

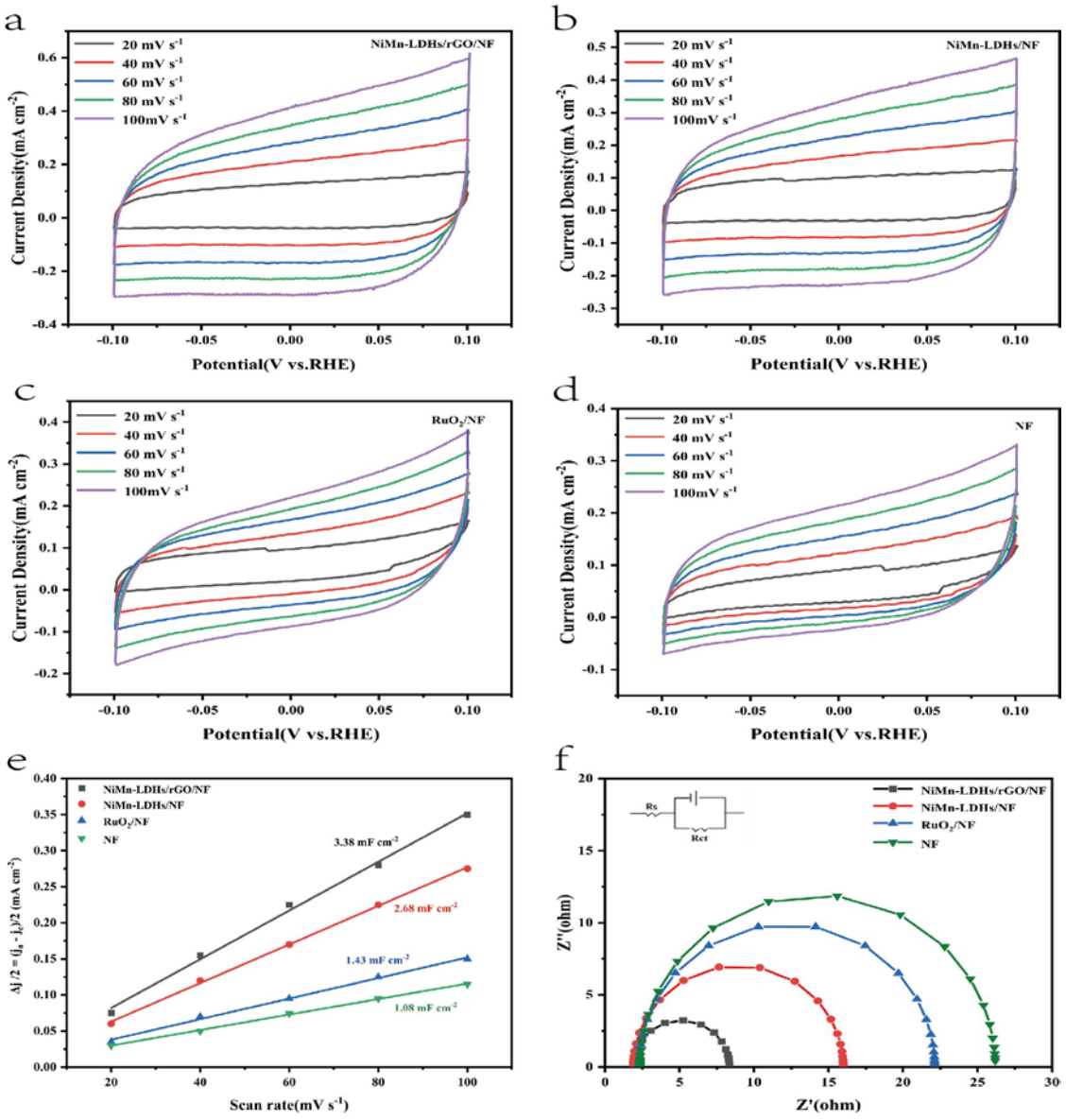

Figure 7. (a-d) CV curves in 1.0 M KOH, (e) linear plot of capacitance vs. scan rate and (f) Nyquist plots for NiMn-LDHs/rGO/NF, NiMn-LDHs/NF, RuO_2/NF and NF. .

The electrochemical active surface area (ECSA) of the investigated catalysts were estimated via a simple CV scanning (see **Figure 7a-d**) for better evaluating the number of catalytic active sites. The slope of Δj/2 vs. Scan rate is known to be equal to the value of Cdl (Cdl is the double layer capacity), which has a linear relationship with ECSA[14,15]. From the fitted lines shown in **Figure 7e**, it is clear that the Cdl of the investigated catalysts increases gradually in the following order NF <RuO_2 (1.43 mF cm^{-2})/NF<NiMn-LDHs/NF (2.68 mF cm^{-2}) < NiMn-LDHs/rGO/NF (3.38 mF cm^{-2}). Because of its largest value of ECSA, the NiMn-LDHs/rGO/NF composite catalyst should be of the largest number of active sites, which is one of the crucial factors that determines its excellent OER performance.

Since the Tafel slope obtained directly from the LSV curve is affected by the solution impedance and the material internal resistance, it reflects the overall OER kinetics of the catalyst, but cannot be used to analyze the OER mechanism of the catalyst. Thus, EIS was applied to obtain information on charge transfer between the electrolyte and the electrode surface to elucidate the kinetic differences of the catalysts investigated in this work. From the EIS spectra shown in **Figure 7f**, it can be seen that

the NiMn-LDHs/rGO/NF composite electrode exhibits the smallest diameter among the Nyquist semicircles, which indicates that the electrode has the lowest charge transfer resistance (Rct). Since Rct influences the conductivity of the electrode and thus electron transfer in the electrochemical reaction process, it is expected that the NiMn-LDHs/rGO/NF electrode also has the quickest charge-transfer rate during reaction process and hence the highest electrochemical activity among the investigated electrodes. Moreover, the catalysts which possessed a layered atomic structure demonstrate a greatly decreased charge transfer resistance relative to RuO_2/NF, suggesting that the atomic structure greatly influences the electronic conductivity of the catalysts.

3. Materials and Methods

3.1 Material

$Ni(NO_3)_2 \cdot 6H_2O$, $MnCl_2$ and RuO_2 were obtained from Aladdin Bio-Chem Technology Co. Ltd. Potassium permanganate was acquired from Liaoning Quanrui Reagent Co, and urea from TJCCR Co. Ltd. Nickel foam, Acetone and hydrochloric acid were obtained from Aladdin Bio-Chem Technology Co. Ltd. All of the chemicals used in this work were of analytical grade and used without further purification.

3.2 Preparation of the self-supporting NiMn-LDHs/rGO/NF composite electrode

The procedure for the preparation the self-supporting NiMn-LDHs/rGO/NF composite electrode was depicted in **Figure 8**. GO was prepared by oxidation of graphite powder using Hummers' method. A mixture containing 0.12 mmol $Ni(NO_3)_2 \cdot 6H_2O$, 0.04 mmol $MnCl_2$ and 0.72 mmol urea was dissolved in 20 mL of deionized water, and then 10 mL of 0.2 mg/mL rGO solution was added. After ultrasonication for 40 minutes, the solution along with a piece of NF (10 x 10 cm), which was ultrasonically cleaned in 2 M HCl, acetone, ethanol and deionized water, respectively, and then dried at 60° for 5 hours, was poured into a 50 mL Teflon lining autoclave and kept at 140° for 10 hours. When the autoclave was cooled naturally to room temperature, the product was collected and washed with large amount of deionized water to get rid of the adsorbed substances. The self-supporting NiMn-LDHs/rGO/NF composite electrode was achieved after drying of the product in an oven at 60° for 3 hours. The self-supporting NiMn-LDHs/NF composite electrode was prepared in the same procedure without the addition of rGO. For comparison, the RuO_2/NF electrode was also prepared following the method reported previously[28].

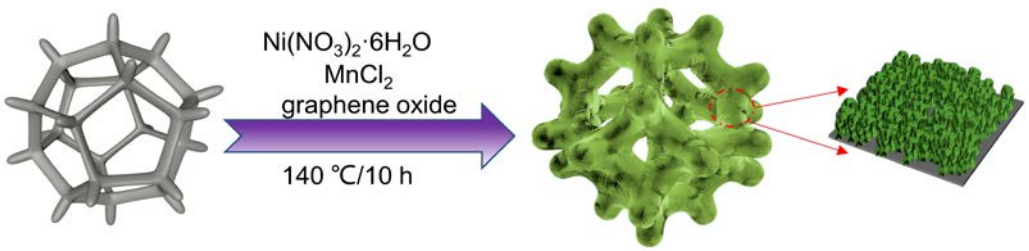

Figure 8. Schematic description of the procedure for the preparation of NiMn-LDHs/rGO/NF composite catalyst.

 doi:10.20944/preprints202305.0210.v1

3.3 Characterization

The morphology of the catalysts was observed by scanning electron microscopy (SEM, QUANTA 200S, FEI, Eindhoven, The Netherlands) and transmission electron microscopy (TEM, JEM2100, JEOL, Tokyo, Japan). The crystalline phase of the catalyst was obtained by X-ray diffraction (XRD, D8 Advance, Bruker, Berlin, Germany) at 40 kV and 200 mA operating conditions in the 2θ range from 10 to 70. The elemental composition and oxidation state of the catalysts were analyzed by X-ray electron spectroscopy (XPS, KRATOS, Stratford, UK). Raman scattering spectra were collected by a Jobin Yvon (Palaiseau, France) HR 800 micro-Raman spectrometer with 532 nm excitation. Fourier transform infrared spectra (FT-IR) were recorded by a Perkin Elmer (Waltham, MA, USA) Spectrum 100FT-IR spectrometer with background correction by referring KBr pellets.

All of the electrochemical tests were conducted on an SP-300 electrochemistry workstation (Bio-Logic, Seyssinet-Pariset, France) in a three-electrode system. The reference electrode was an Hg/HgO one, and the counter electrode was a sheet of platinum. The investigated electrodes including NiMn-LDHs/rGO/NF, NiMn-LDHs/NF, RuO_2/NF and NF were used as working electrodes, respectively. The electrolyte was a solution of 1 mol L^{-1} KOH, which was bubbled with pure oxygen for 30 min to maintain oxygen saturation. The potentials achieved were converted into reversible hydrogen ones by the following equation.

$$E_{RHE} = E_{Hg/HgO} + 0.059 \times pH + 0.098$$

Prior to data collection, cyclic voltammetry (CV) scanning was performed for 30 min at a scanning rate of 100 mV s^{-1} to fully activate the working electrode. CV measurements were conducted in the range of -0.1 V to 0.1 V (vs. Hg/HgO electrode). Linear scan voltammetry (LSV) polarization curves in the voltage range of 0 to 1 V for OER reactions were obtained at a scanning rate of 5 mV s^{-1} in a solution of 1 mol L^{-1} KOH. Electrochemical impedance spectroscopy (EIS) was performed over a frequency range spanning from 100 kHz to 0.01 Hz. The transient photocurrent-time curves (I-t) were applied to assess the stability of the prepared materials. The value of Cdl (Cdl is the double layer capacity) equals to the slope of the fitted straight line of current density difference dependence of scanning rate, which has a linear relationship with the interfacial area between the electrode surface and the electrolyte. Thus, ECSA can be extracted from the electrochemical double layer capacitance (Cdl) by

$$ECSA = Cdl/Cs$$

Herein, Cs represents the specific capacitance, which is 0.040 mF cm^{-2} in a solution of 1.0 M KOH as reported previously [1].

4. Conclusions

An effective OER electrocatalyst was produced by anchoring the composite of NiMn-LDHs ultrathin nanosheets and thin-layered reduced graphene oxide on the skeleton of nickel foam via a facile one-pot hydrothermal method. A series of electro-chemistry experiments confirmed the excellent OER catalytic performance of the self-supporting NiMn-LDHs/rGO/NF composite electrode. In comparison with those of the self-supporting NiMn-LDHs/NF composite electrode, the overpotential at 10 mA cm^{-2} and Tafel slope of the self-supporting NiMn-LDHs/rGO/NF composite electrode are deduced about 80 mV and 25 mV dec^{-1}, respectively, in a solution of 1 mol L^{-1} KOH. The interactions between NiMn-LDHs and rGO are responsible for the largely enhanced electrocatalytic performance. On one hand, ultrathin NiMn-LDHs sheets reduce the graphitization degree of rGO, whereas thin-layered rGO also effectively prevents the re-aggregation of ultrathin NiMn-LDHs sheets. On the other hand, quick charge transfer from ultrathin NiMn-LDHs sheets to thin-layered rGO occurs at their interfaces, resulting in the rise both for the binding energy and for the oxidation state of Ni and Mn atoms. Thus, it is expected that the conductivity and chemically active sites are accordingly increased, which is favorable to the enhancement of the electrocatalytic performance of the self-supporting NiMn-LDHs /rGO/NF composite electrode in OER reaction.

Author Contributions: Conceptualization, J.W. and Y.L.; methodology, J.W.; validation, J.W.; formal analysis, J.W. and Y.L.; investigation, J.W.; resources, Y.L.; data curation, Q.Z. and Y.L.; writing—original draft

preparation, J.W.; writing—review and editing, J.W. and Y.L.; supervision, Y.L. All authors have read and agreed to the published version of the manuscript.

Funding: Not available.

Data Availability Statement: Not available.

Conflicts of Interest: There are no conflict to declare.

References

1. Huo, J. M.; Wang, Y.; Yan, L. T.; et al. In situ semi-transformation from heterometallic MOFs to Fe-Ni LDH/MOF hierarchical architectures for boosted oxygen evolution reaction. *Nanoscale*, **2020**, 12(27): 14514-23.
2. Arahad, N.; Usman, M.; Adnan, M.; et al. Nanoengineering of NiO/MnO_2/GO Ternary Composite for Use in High-Energy Storage Asymmetric Supercapacitor and Oxygen Evolution Reaction (OER). *Nanomaterials-Basel*, **2023**, 13(1).
3. Luo, Y.; Wu, Y. H.; Wu, D. H.; et al. NiFe-Layered Double Hydroxide Synchronously Activated by Heterojunctions and Vacancies for the Oxygen Evolution Reaction. *ACS. Appl. Mater Inter.*, **2020**, 12(38): 42850-8.
4. Kim, B.; Chio, S. I.; Lee, K. Y.; In situ/operando structural tracking of Ni-Fe LDH. *Matter-Us*, **2022**, 5(10).
5. Zhou, Y., Zhang, W. B. A., Hu, J. L., et al. Inherent Oxygen Vacancies Boost Surface Reconstruction of Ultrathin Ni-Fe Layered-Double-Hydroxides toward Efficient Electrocatalytic Oxygen Evolution. *ACS Sustain Chem Eng*, **2021**, 9(21): 7390-9.
6. Chen, C. ; Tuo, Y. X.; Lu, Q.; et al. Hierarchical trimetallic Co-Ni-Fe oxides derived from core-shell structured metal-organic frameworks for highly efficient oxygen evolution reaction. *Appl Catal B-Environ*, **2021**, 287.
7. Du, Y.; Liu, D. P.; Li, T. Z.; et al. A phase transformation-free redox couple mediated electrocatalytic oxygen evolution reaction. *Appl Catal B-Environ*, **2022**, 306.
8. Kazakova, M. A.; Morales, D. M.; Andronescu C., et al. Fe/Co/Ni mixed oxide nanoparticles supported on oxidized multi-walled carbon nanotubes as electrocatalysts for the oxygen reduction and the oxygen evolution reactions in alkaline media. *Catal Today*, **2020**, 357: 259-68.
9. Li, Y.; Wu, Y. Y.; Yuan, M. K.; et al. Operando spectroscopies unveil interfacial FeOOH induced highly reactive beta-Ni(Fe)OOH for efficient oxygen evolution. *Appl Catal B-Environ*, **2022**, 318.
10. Lin, Y. P.; Fan, X. M.; Huang, M. Q.; et al. Preferential Co substitution on Ni sites in Ni-Fe oxide arrays enabling large-current-density alkaline oxygen evolution. *Chem Sci*, **2022**, 13(24): 7332-40.
11. Pan, J. J.; Hao, S. Y.; Zhang, X. W.; et al. In situ growth of Fe and Nb co-doped beta-Ni(OH)(2)nanosheet arrays on nickel foam for an efficient oxygen evolution reaction. *Inorg Chem Front*, **2020**, 7(18): 3465-74.
12. Chen, Z.; Wang, Z.; Cai, R.; et al. NiMn compound nanosheets for electrocatalytic water oxidation: effects of atomic structures and oxidation states [J]. *Nanoscale*, **2020**, 12.
13. Wang, Y; Liu, X. H.; Zhang, N; et al. Cobalt-doped Ni-Mn layered double hydroxide nanoplates as high-performance electrocatalyst for oxygen evolution reaction [J]. *Appl Clay Sci*, **2018**, 165: 277-83.
14. An, L.; Zhang, H.; Zhu, J. M.; et al. Balancing Activity and Stability in Spinel Cobalt Oxides through Geometrical Sites Occupation towards Efficient Electrocatalytic Oxygen Evolution. *Angew Chem Int Edit*, **2022**.
15. Salmanion, M.; Kondov, I.; Vandichel, M.; et al. Surprisingly Low Reactivity of Layered Manganese Oxide toward Water Oxidation in Fe/Ni-Free Electrolyte under Alkaline Conditions. *Inorg Chem*, **2022**, 61(4): 2292-306.
16. Sun, J.; Du, L.; Sun, B. Y.; et al. A bifunctional perovskite oxide catalyst: The triggered oxygen reduction/evolution electrocatalysis by moderated Mn-Ni co-doping. *J Energy Chem*, **2021**, 54: 217-24.
17. Zhang, Y.; Zeng, Z. Y.; Ho, D. R.. Mn dopant induced high-valence $Ni^{(3+)}$ sites and oxygen vacancies for enhanced water oxidation. *Mater Chem Front*, **2020**, 4(7): 1993-9.
18. Sapner, V. S.; Mulik, B. B.; Digraskar, R, et al. Enhanced oxygen evolution reaction on amine functionalized graphene oxide in alkaline medium. *RSC Adv*, **2019**, 9(12): 6444-51.
19. Yaqoob, L.; Noor, T.; Iqbal, N.; et al. Nanocomposites of cobalt benzene tricarboxylic acid MOF with rGO: an efficient and robust electrocatalyst for oxygen evolution reaction (OER). *Renewable Energy*, **2020**, 156: 1040-54.
20. Mao, S.; Wen, Z.; Huang, T.; et al. High-performance bi-functional electrocatalysts of 3D crumpled graphene–cobalt oxide nanohybrids for oxygen reduction and evolution reactions. *Energy & Environmental Science*, **2014**, 7(2): 609-16.

21. Jahan, M.; Liu, Z.; Loh, K. P.. A Graphene oxide and copper-centered metal organic framework composite as a tri-functional catalyst for HER, OER, and ORR. *Advanced Functional Materials*, **2013**, 23(43): 5363-72.
22. Han, X.; Suo, N.; Chen, C.; et al. Graphene oxide guiding the constructing of nickel-iron layered double hydroxides arrays as a desirable bifunctional electrocatalyst for HER and OER. *International Journal of Hydrogen Energy*, **2019**, 44(57): 29876-88. 37.
23. Mooni, S. P., Kondamareddy, K. K., Li, S. L., et al. Graphene oxide decorated bimetal (MnNi) oxide nanoflakes used as an electrocatalyst for enhanced oxygen evolution reaction in alkaline media. *Arab J Chem*, **2020**, 13(3): 4553-63.
24. Ma, W.; Ma, R. Z.; Wu, J. H.; et al. Development of efficient electrocatalysts via molecular hybridization of NiMn layered double hydroxide nanosheets and graphene [J]. *Nanoscale*, **2016**, 8(19): 10425-32.
25. Lu, Y. T.; Wu, J. Y.; Lin, Z. X.; et al. Enhanced oxygen evolution performance of spinel $Fe_{0.1}Ni_{0.9}Co_2O_4$/Activated carbon composites [J]. *Electrochim Acta*, **2019**, 326.
26. Yin, P. Q.; Wu, G.; Wang, X. Q.; et al. NiCo-LDH nanosheets strongly coupled with GO-CNTs as a hybrid electrocatalyst for oxygen evolution reaction. *Nano Res*, **2021**, 14(12): 4783-8.
27. Zhang, Y.; Cheng, C. Q.; Kuai, C. G.; et al. Unveiling the critical role of the Mn dopant in a $NiFe(OH)_{(2)}$catalyst for water oxidation. J. Materials Chem. A, **2020**, 8(34): 17471-6.
28. Lin, H. Y.; Wang, X. L.; Wang, T.; et al. A facile, green and time-saving method to prepare partially crystalline NiFe layered double hydroxide nanosheets on nickel foam for superior OER catalysis [J]. *J Alloy Compd*, **2020**, 844.